



Dalton
Transactions

**Three derivatives of phenacyldiphenylphosphine oxide:
Influence of aromatic and alkyl substituents on the
luminescence sensitization of four Ln(NO₃)₃ salts**

Journal:	<i>Dalton Transactions</i>
Manuscript ID	DT-ART-10-2023-003556.R1
Article Type:	Paper
Date Submitted by the Author:	29-Dec-2023
Complete List of Authors:	Sands, Georgia; Grand Valley State University, Chemistry Cook, Alyssa; Grand Valley State University, Chemistry Delabbio, Angelina; Grand Valley State University, Chemistry Fuhrer, Timothy; Radford University Bailey, Matthew; Northwestern University Leach, Erin; Grand Valley State University, Chemistry Purosky, Isabella; Grand Valley State University, Chemistry Biros, Shannon; Grand Valley State University, Chemistry

SCHOLARONE™
Manuscripts

Three derivatives of phenacyldiphenylphosphine oxide: Influence of aromatic and alkyl substituents on the luminescence sensitization of four Ln(NO₃)₃ salts

Georgia G. Sands,^a Alyssa K. Cook,^a Angelina Delabbio,^a Tim Fuhrer,^b Matthew D. Bailey,^c Erin G. Leach,^a Isabella R. Purosky,^a Shannon M. Biros^{a*}

^aDepartment of Chemistry, Grand Valley State University, Allendale, MI 49401, USA

^bDepartment of Chemistry, Radford University, Radford, VA 24142, USA

^cDepartment of Chemistry, Northwestern University, Evanston, IL 60208, USA

*Corresponding Author: Shannon M. Biros (biross@gvsu.edu)

Abstract

A series of four β -carbonylphosphine oxide compounds have been synthesized, and their complexes with the nitrate salts of Sm³⁺, Eu³⁺, Tb³⁺ and Dy³⁺ have been characterized in solution and in the solid state. Analysis of the complexes using IR and NMR suggests that metal-ligand binding occurs mainly through the phosphine oxide group of the ligand, with some involvement of the carbonyl group. All 16 complexes luminesce in solutions of acetonitrile, albeit with varying degrees of intensity. The highest quantum yield values obtained for this series are those where the ligand contains an aryl carbonyl group paired with an electron rich phosphine oxide group (29.8 and 11% for the Tb³⁺ and Eu³⁺ complexes, respectively). In contrast, the longest emission lifetime values were found for complexes where the ligand contains a bulky substituent on the carbonyl group paired with an electron rich phosphine oxide (1.86, 1.402, 0.045 ms for the Tb³⁺, Eu³⁺ and Sm³⁺ complexes, respectively).

Introduction

1. Background – some uses of lanthanide metals and the β -carbonylphosphine oxide group

Lanthanide (Ln) metals have been incorporated into a wide array of chemical reagents, materials and devices due to their unique properties.^{1,2} Synthetic chemists have used Kagan's reagent (SmI₂)³ for over forty years as a powerful reducing agent, and recent developments from Schelter and co-workers have demonstrated the usefulness of Ce(IV) as an oxidant for C(sp³)-H

bonds.⁴ Magnetic resonance images can be enhanced through the use of contrast agents that incorporate Gd^{3+} ,^{5,6} and light emitting diodes exploit the luminescence of Ln metals such as $Eu^{2+/3+}$ and Tb^{3+} to produce vibrant red and green light.^{7,8} The unpaired electrons present in many Ln ions have made them great candidates for use in single molecule magnets (Dy^{3+})^{9,10} that could find use in quantum computing,¹¹ as well as in permanent magnets (e.g. $Nd_2Fe_{14}B$)¹² found in, for instance, hybrid car batteries.

In many of the applications described above, the metal is complexed by an organic ligand or organic polymer that enhances the properties of the Ln ion. Since Ln metals bind well with hard, anionic donors, many organic ligands used in Ln coordination compounds contain at least one phosphine oxide, carbonyl, or alcohol group. For instance, the well-known CMPO (carbamoylmethylphosphine oxide) motif is part of a ligand that is an active component in the TRUEX process for the treatment of spent nuclear fuel and features two of these groups as a β -amidophosphine oxide.¹³ This bidentate ligand, which features both a carbonyl and a phosphine oxide group, represents an attractive binding group for Ln metals. The phosphine oxide bond is quite polarized and is stable under many different types of conditions (e.g. acidic, basic, oxidizing) while the carbonyl group is easy to derivatize with any number of desired substituents. Our group is interested in utilizing the Ln-binding ability of the β -carbonylphosphine oxide group to create new organic ligands that are capable of binding to and sensitizing the luminescence of lanthanide ions.

As part of our work in this area we studied the aryl-substituted phosphine oxide compound **1** that bears a β -aryl ketone (Figure 1). In 2017 we reported the solid-state (IR, X-Ray diffraction) and solution (NMR, luminescence) characterization of β -ketophosphine oxide **1** complexed with a selection of $Ln(NO_3)_3$ salts ($Ln = Sm, Eu, Gd, Tb$ and Dy).¹⁴ Compound **1** formed 1:2 $Ln(NO_3)_3$ -ligand complexes with each of these metals in the solid state (as determined by X-Ray diffraction), where the ligand was bound to the metal in a monodentate manner through the phosphine oxide group. In the case of the $[Eu(\mathbf{1})_2(NO_3)_3]$ complex, a crystal structure was also obtained where the ligand was bound to the metal in a bidentate manner through both the carbonyl and phosphine oxide groups. Lastly, compound **1** was able to sensitize the metal-centered emission of the Ln(III) metals Sm, Eu, Tb and Dy in solutions of acetonitrile with respectable quantum yields (Figure 1).

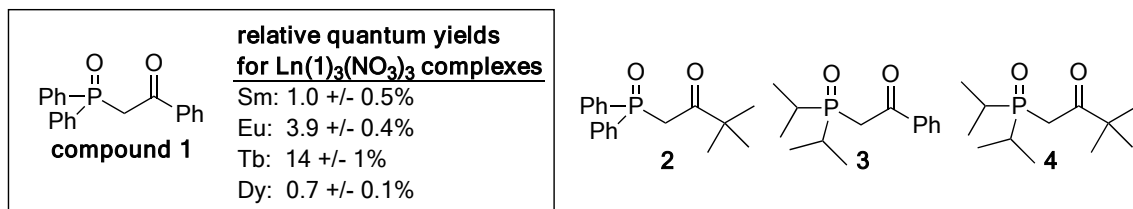


Figure 1. Structures of compounds investigated in this work, and quantum yield values for compound **1** (2.0 mM complex in CH₃CN, 1:3 Ln-ligand ratio).

When we consider the two functional groups of ligand **1**, the carbonyl group, especially when substituted with an aromatic ring, is known to be an efficient antenna for the sensitization of lanthanide luminescence.² The ability of the phosphine oxide group to facilitate this sensitization process has also been investigated, but to a lesser extent.¹⁵⁻²² Our goal with this work was to tease out the role of each functional group of the ligand - the carbonyl vs. the phosphine oxide - in both the Ln(III) binding and luminescence properties of its resultant complexes. To investigate this, we prepared the three derivatives **2-4** shown in Figure 1, where each aromatic group was isolated in turn by its replacement with alkyl groups. Our hypothesis at the outset of this work was that the aryl carbonyl group would dominate the luminescence sensitization ability of these ligands, thus compound **3** would demonstrate sensitization properties similar to compound **1**. We then proposed that compounds **2** and **4**, having only an alkyl-substituted carbonyl, would be poor sensitizers for the luminescence of the four Ln(III) metals investigated here.

2. Mechanism of the antenna effect for lanthanide luminescence – an abbreviated description

First reported by Weissman in 1942,²³ the generally accepted mechanism for the antenna effect is that the ligand is excited upon absorption of light to a singlet excited state, at which time it can undergo intersystem crossing (ISC) to the triplet excited state.^{24, 25} It is also generally accepted that energy transfer from the triplet excited state of the ligand to an *f* excited state on the metal is the dominant pathway in this process, although population of the metal from the ligand's singlet excited state has been observed. It has been stated that the ideal energy difference between the ligand's excited state and the metal's accepting *f* excited state is between 2,500 and 4,000 cm⁻¹, although exceptions to this have also been observed.²⁵ From each of these excited states the ligand can relax either by emitting light or by non-radiative decay pathways. If the energy of the ligand's populating state and the metal's accepting state is close enough in

energy (less than $\sim 5000\text{ cm}^{-1}$) back transfer can occur where the ligand's excited state is repopulated. An abbreviated Jablonski Diagram depicting this process is shown in Figure 2. We refer the reader to a number of excellent reviews and books that describe this process in more detail.^{2, 7, 26}

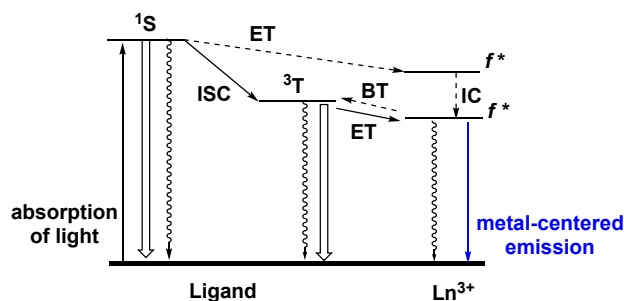


Figure 2. An abbreviated Jablonski diagram depicting the antenna effect with Ln ions. The singlet and triplet states of the ligand are denoted with 1S and 3T , respectively. Open arrows represent fluorescence (from 1S) and phosphorescence (3T), and squiggly arrows denote non-radiative decay pathways. ISC is intersystem crossing, ET is energy transfer, BT is back-energy transfer, IC is internal conversion, and f^* are excited states of the Ln ion. Only the lowest energy vibrational states are shown.

Experimental

General considerations

All chemicals (including deuterated solvents) were purchased from Sigma-Aldrich or Strem Chemical and used without further purification. NMR spectral data (1H , ^{13}C , ^{31}P) were recorded on a JEOL ECZS 400 NMR spectrophotometer. For NMR spectra, chemical shifts are expressed as parts per million (δ) relative to $SiMe_4$ (TMS, $\delta = 0$) for 1H and ^{13}C data, and H_3PO_4 ($\delta = 0$) for ^{31}P data. Both ^{13}C and ^{31}P NMR spectra were obtained as proton-decoupled data. IR spectra were acquired neat on a Jasco 4100 FTIR. Elemental (CHN) analyses were performed by Atlantic Microlab Inc., Norcross, GA; all CHN percentages calculated for lanthanide complexes assume two phosphine oxide ligands + $Ln(NO_3)_3$ + residual water/solvents as indicated. Low resolution mass spectrometry data were acquired on an Advion Expression-L Compact Mass Spectrometer in ESI mode (direct introduction). High resolution mass spectrometry data were acquired at the Lumigen Instrument Center at Wayne State University. Luminescence data were recorded on a

Horiba Fluoromax 4 fluorimeter, and absorption spectra were collected using a Shimadzu UV-2450 spectrophotometer.

Synthesis.

Ligand 1. This preparation is an improved method from what was described in our original report.¹⁴ A round bottom flask was charged with 2-bromoacetophenone (0.86 g, 4.3 mmol) and ethyl diphenylphosphinite (1.0 g, 0.94 mL, 4.3 mmol) and left open to air. The reaction was heated to 160 °C for two hours with an oil bath and was allowed to cool to room temperature to give an orange, viscous gel. The product was triturated three times with diethyl ether (10 mL total) and three times with ethyl acetate (15 mL total). The product was placed under high vacuum overnight to give the pure product as a white powder (0.84 g, 2.6 mmol, 61%). All characterization data for this ligand was identical to previous reports of this compound from our group.¹⁴

Ligand 2. Bromopinacolone (0.41 g, 0.31 mL, 2.3 mmol) and ethyl diphenylphosphinite (1.07 g, 0.5 mL, 2.3 mmol) were added to a round bottom flask. The reaction was heated to 160 °C for two hours with an oil bath. The reaction was allowed to cool to room temperature to give a fine white powder as the pure product (0.703 g, 100% yield). If impurities were generated in this reaction, they were removed by trituration of the crude product with diethyl ether (3 x 5 mL). ¹H NMR (CDCl₃, 400 MHz): δ 7.92-7.20 (m, 10H), 3.67 (d, *J*_{HP} = 16 Hz, 2H), 1.05 (s, 9H, t-butyl); ¹³C NMR (CDCl₃, 100 MHz): δ 208.4 (d, *J*_{CP} = 7 Hz), 133.1 (s), 132.1 (s), 131.2 (d, *J*_{CP} = 10 Hz), 128.6 (d, *J*_{CP} = 12 Hz), 45.4 (s), 40.3 (*J*_{CP} = 63 Hz), 26.0 (s); ³¹P (CDCl₃, 161 MHz): δ 29.0 (s); FT-IR (ν, cm⁻¹): 1187 (P=O), 1700 (C=O); ESI-HRMS (M⁺, *m/z*): calculated of C₁₈H₂₂O₂P: 301.3444, found 301.1342; UV-VIS (4.0 mM, CH₃CN): λ_{max} 294 nm.

Ligand 3. Chlorodiisopropylphosphine (2.5 g, 2.6 mL, 16.4 mmol) and 2-bromoacetophenone (3.3 g, 16.4 mmol) were combined in a 50 mL round bottom flask. The reaction mixture was stirred for two hours and left to sit for two days under nitrogen to give an orange, translucent gel. The mixture was then dissolved in chloroform (15 mL) and added dropwise to a stirring solution of saturated NaHCO₃ (60 mL). The layers were separated, the aqueous layer was extracted with chloroform two times (15 mL each), and the combined organic layers were then washed with

saturated NaHCO_3 (20 mL). The organic layer was dried with anhydrous magnesium sulfate and concentrated under reduced pressure to give an oil. This crude product was purified with a column of silica gel (1% MeOH in CHCl_3) to give a nearly pure product that sometimes contained a small impurity. If present, the impurity was removed via Kugelrohr distillation (40 mmHg, 60-65 °C) to leave behind the pure product as a light-yellow oil (1.87 g, 45 % yield). ^1H NMR (CDCl_3 , 400 MHz): δ 8.06-7.48 (m, 5H), 3.55 (d, $J_{\text{HP}} = 12$ Hz, 2H), 2.21 (m, 2H), 1.22 (m, 12H); ^{13}C NMR (CDCl_3 , 75 MHz): δ 194.9 (s), 137.2 (s), 133.6 (s), 129.2 (s), 128.4 (s), 37.5 (d, $J_{\text{CP}} = 33.8$ Hz), 27.0 (d, $J_{\text{CP}} = 49.8$ Hz), 16.2 (d $J_{\text{CP}} = 32.25$ Hz); ^{31}P (CDCl_3 , 161 MHz): δ 56.3 (s). FT-IR (cm^{-1}): ν 1178 (P=O), 1669 (C=O); ESI-HRMS (MH^+ , m/z): calculated of $\text{C}_{14}\text{H}_{22}\text{O}_2\text{P}$: 253.1357; found: 253.1347; UV-VIS (4.0 mM, CH_3CN): λ_{max} 289 nm.

Ligand 4. Chlorodiisopropylphosphine (5.0 g, 32.8 mmol) and bromopinacolone (5.86 g, 32.8 mmol) were combined in a 50 mL Schlenk flask and the flask was purged with argon gas. The flask was sealed, and the reaction was stirred for two days to give a mixture that had stopped stirring due to the presence of a thick white solid. The mixture was then dissolved in chloroform (30 mL) and added dropwise to a stirring solution of saturated NaHCO_3 (120 mL). The layers were separated, the aqueous layer was extracted with chloroform two times (20 mL each), and the combined organic layers were then washed with saturated NaHCO_3 (20 mL). The organic layer was dried with anhydrous magnesium sulfate and concentrated under reduced pressure to give a light tan liquid. The oil was purified with two silica gel columns (2.5% MeOH in CH_2Cl_2 , $R_f = 0.2$, then 10% MeOH in EtOAc, $R_f = 0.3$) to give a nearly pure product with a small impurity. This impurity was removed via Kugelrohr distillation (40 mmHg, 60-65 °C) to leave behind the pure product as a light-yellow oil (596 mg, 7.8% yield). ^1H NMR (CDCl_3 , 400 MHz): δ 3.12 (d, $J_{\text{HP}} = 16$ Hz, 2H), 2.23 (m, 2H), 1.20 (m, 8H), 1.18 (s, 9H); ^{13}C NMR (CDCl_3 , 75 MHz): δ 210.5 (s), 45.5 (s), 34.2 (d, $J_{\text{CP}} = 38.6$ Hz), 26.8 (d, $J_{\text{CP}} = 48.9$ Hz), 26.5 (s), 16.3 (d, $J_{\text{CP}} = 36.0$ Hz); ^{31}P (CDCl_3 , 161 MHz): δ 57.0 (s); FT-IR (cm^{-1}): ν 1172 (P=O), 1698 (C=O). ESI-HRMS (MH^+ , m/z): calculated of $\text{C}_{12}\text{H}_{26}\text{O}_2\text{P}$: 233.1670; found: 233.1659; UV-VIS (4.0 mM, CH_3CN): λ_{max} 290 nm.

Complexes with Ligand 1.

General procedure. Ligand **1** (80 mg, 0.25 mmol) was dissolved in 15 mL acetonitrile in a round bottom flask. A half-molar equivalent of $\text{Ln}(\text{NO}_3)_3$ hydrate (0.12 mmol) was added as a solid. The resulting mixture was stirred for 30 minutes. The acetonitrile was then removed under reduced pressure, resulting in a clear oil. The complexes were triturated three times with diethyl ether (10 mL total) leaving an off-white powder (around 50% yield). Characterization data for these complexes was consistent with the previous report from our group.¹⁴

Complexes with Ligand 2.

General procedure. Ligand **2** (75 mg, 0.25 mmol) was dissolved in 15 mL acetonitrile in a round bottom flask. A half-molar equivalent of $\text{Ln}(\text{NO}_3)_3$ hydrate (0.12 mmol) was added as a solid. The resulting mixture was stirred for 30 minutes. The acetonitrile was then removed under reduced pressure, resulting in a clear oil. The complexes were triturated three times with diethyl ether (10 mL total) leaving a clear, flaky solid (around 50% yield).

[Sm(2)₂(NO₃)₃] complex: ¹H NMR (CD₃CN, 400 MHz): δ 8.14-7.43 (m, 10H), 4.31 (d, $J_{\text{HP}}=12$ Hz, 2H), 0.73 (s, 9H); ¹³C NMR (CD₃CN, 100 MHz): δ 210.9 (s, C=O), 133.3 (s), 131.6 (d, $J_{\text{CP}}=11$ Hz), 130.2 (s), 129.1 (d, $J_{\text{CP}}=10$ Hz), 45.1 (s), 38.1 (d, $J_{\text{CP}}=70$ Hz); ³¹P NMR (CD₃CN, 161 MHz): δ 37.5 (s); FT-IR (ν, cm⁻¹): 1702 (C=O free), 1684 (C=O bound), 1156 (P=O); CHN analysis calculated (found): C 46.14 (45.17), H 4.54 (4.75), N 4.48 (4.27); ESI-LRMS (M^{2+} , m/z) calcd for $[\text{Sm}(\text{C}_{18}\text{H}_{22}\text{O}_2\text{P})_2(\text{NO}_3)]^{2+}$: 405.6, 407.1, found 405.1, 407.2.

[Eu(2)₂(NO₃)₃] complex: FT-IR (ν, cm⁻¹): 1704 (C=O free), 1671 (C=O bound), 1154 (P=O); CHN analysis calculated (found): C 46.07 (45.96), H 4.51 (4.25), N 4.48 (4.38); ESI-LRMS (M^{2+} , m/z): calcd for $[\text{Eu}(\text{C}_{18}\text{H}_{22}\text{O}_2\text{P})_2\text{NO}_3]^{2+}$: 406.6, 407.6, 408.1, found: 405.2, 407.2, 408.1.

[Dy(2)₂(NO₃)₃] complex: FT-IR (ν, cm⁻¹): 1708 (C=O free), 1670 (C=O bound), 1154 (P=O); CHN analysis calculated (found): C 45.55 (44.43), H 4.46 (4.68), N 4.43 (4.46); ESI-LRMS (M^+ , m/s) calcd for $[\text{Dy}(\text{C}_{18}\text{H}_{22}\text{O}_2\text{P})_2(\text{NO}_3)_2]^+$: 888.16, 887.16, 886.16, found 888.2, 887.4, 886.2.

[Tb(2)(NO₃)₃] complex: FT-IR (ν , cm⁻¹): 1708 (C=O free), 1671 (C=O bound), 1154 (P=O); CHN analysis calculated (found): C 45.73 (44.42), H 4.48 (4.72), N 4.44 (4.13); ESI-LRMS (M⁺, m/z) calcd of [Tb(C₁₈H₂₂O₂P)₂(NO₃)₂]⁺: 883.2, found 883.1.

Complexes with ligand 3.

General procedure. Ligand **3** (200 mg, 0.793 mmol) was dissolved in 20 mL acetonitrile in a round bottom flask. A half-molar equivalent of Ln(NO₃)₃ hydrate (0.396 mmol) was added as a solid. The resulting mixture was stirred for 30-60 minutes at room temperature. The acetonitrile was then removed under reduced pressure, resulting in a clear oil. The complexes were triturated three times with diethyl ether (10 mL total) to give a white amorphous gel, which when placed under high vacuum turned into a white foam (75-85% yield).

[Sm(3)₂(NO₃)₃] complex: ¹H NMR (CD₃CN, 400 MHz): δ 7.74 (d, $J=8.0$ Hz, 2H), 7.61 (t, $J=8.0$ Hz, 1H), 7.42 (t, $J=8.0$ Hz, 2H), 4.30 (d, $J_{HP}=16$ Hz, 2H), 2.87 (m, 2H), 1.55 (dd, $J_{HP,HH}=16, 8$ Hz, 6H), 1.43 (dd, $J_{HP,HH}=16, 8$ Hz, 6H); ¹³C NMR (CD₃CN, 100 MHz): δ 197.3 (d, $J_{CP} = 4$ Hz), 135.7 (d, $J_{CP} = 3$ Hz), 135.2 (s), 129.1 (d, $J_{CP} = 4$ Hz), 32.9 (d, $J_{CP} = 54$ Hz), 26.5 (d, $J_{CP} = 65$ Hz), 15.4 (*apparent* s), 14.9 (d, $J_{CP} = 2$ Hz); ³¹P NMR (CD₃CN, 161 MHz): δ 71.0 (s); FT-IR (ν , cm⁻¹): 1674 (C=O free), 1640 (C=O bound), 1107 (P=O); CHN analysis calculated (found) for [Sm(C₁₄H₂₁O₂P)₂(NO₃)₃(H₂O)]: C 39.15 (39.33), H 5.16 (5.06), N 4.89 (4.91); ESI-LRMS (M⁺, m/z) calcd for [Sm(C₁₄H₂₁O₂P)₂(NO₃)₂]⁺: 780.1, 782.1; found 780.2, 782.2.

[Eu(3)₂(NO₃)₃] complex: FT-IR (ν , cm⁻¹): 1673 (C=O bound), 1108 (P=O); CHN analysis calculated (found) for [Eu(C₁₄H₂₁O₂P)₂(NO₃)₃(H₂O)₂]: C 38.28 (38.69), H 5.28 (4.95), N 4.78 (4.91); ESI-LRMS (M⁺, m/z): calcd for [Eu(C₁₄H₂₁O₂P)₂(NO₃)₂]⁺: 781.2, 779.2; found: 781.2, 779.2.

[Dy(3)₂(NO₃)₃] complex: FT-IR (ν , cm⁻¹): 1674 (C=O free), 1638 (C=O bound), 1109 (P=O); CHN analysis calculated (found) for [Dy(C₁₄H₂₁O₂P)₂(NO₃)₃(H₂O)₂]: C 37.82 (38.20), H 5.21 (5.05), N 4.73 (4.88); ESI-LRMS (M⁺, m/z) calcd for [Dy(C₁₄H₂₁O₂P)₂(NO₃)₂]⁺: 792.2, 791.2, 790.2; found 792.1, 790.2, 791.2.

[Tb(3)₂(NO₃)₃] complex: FT-IR (ν , cm⁻¹): 1674 (C=O free), 1637 (C=O bound), 1108 (P=O); CHN analysis calculated (found) for [Tb(C₁₄H₂₁O₂P)₂(NO₃)₃(H₂O)]: C 38.78 (38.47), H 5.11 (4.86), N 4.85 (4.86); ESI-LRMS (M⁺, m/z) calcd of [Tb(C₁₄H₂₁O₂P)₂(NO₃)₂]⁺: 787.2, found 787.3.

Complexes with ligand 4.

General procedure. Ligand **4** (50 mg, 0.215 mmol) was dissolved in 10 mL acetonitrile in a round bottom flask. A half-molar equivalent of Ln(NO₃)₃ hydrate (0.108 mmol) was added as a solid. The resulting mixture was stirred for 60 minutes at room temperature. The acetonitrile was then removed under reduced pressure, resulting in a clear oil which was placed under high vacuum overnight to remove any residual solvents. The complexes were then triturated three times with diethyl ether (10 mL total) to give either a white oil or powder, which when placed under high vacuum turned into a white foam (55-85% yield).

[Sm(4)₂(NO₃)₃] complex: ¹H NMR (CD₃CN, 400 MHz): δ 3.95 (d, J_{HP} =12 Hz, 2H), 2.85 (m, 2H), 1.57 (dd, $J_{HP, HH}$ =14, 8 Hz, 6H), 1.46 (dd, $J_{HP, HH}$ =16, 8 Hz, 6H) 0.99 (s, 9H); ¹³C NMR (CD₃CN, 100 MHz): δ 214.0 (s), 45.5 (s), 31.8 (d, J_{CP} = 58 Hz), 26.4 (d, J_{CP} = 65 Hz), 25.4 (s), 15.2 (d, J_{CP} = 45 Hz); ³¹P NMR (CD₃CN, 161 MHz): δ 70.0 (s); FT-IR (ν , cm⁻¹): 1691 (C=O bound), 1116 (P=O); CHN analysis calculated (found) for [Sm(C₂₄H₅₀O₂P)₂(NO₃)₃(H₂O)₂]: C 34.44 (34.40), H 6.50 (6.30), N 5.02 (5.10); ESI-LRMS (M⁺, m/z) calcd for [Sm(C₁₂H₂₅O₂P)₂(NO₃)₂]⁺: 740.2, 742.2, found 740.3, 742.3.

[Eu(4)₂(NO₃)₃] complex: FT-IR (ν , cm⁻¹): 1691 (C=O bound), 1117 (P=O); CHN analysis calculated (found) for [Eu(C₂₄H₅₀O₂P)₂(NO₃)₃(H₂O)₂]: C 34.37 (34.40), H 6.49 (6.30), N 5.01 (5.10); ESI-LRMS (M⁺, m/z): calcd for [Eu(C₁₂H₂₅O₂P)₂(NO₃)₂]⁺: 741.2, 739.2 found: 741.3, 739.3.

[Dy(4)₂(NO₃)₃] complex: FT-IR (ν , cm⁻¹): 1690 (C=O bound), 1123 (P=O); CHN analysis calculated (found) for [Dy(C₂₄H₅₀O₂P)₂(NO₃)₃(H₂O)]: C 34.68 (34.40), H 6.31 (6.30), N 5.06 (5.10); ESI-LRMS (M⁺, m/z) calcd for [Dy(C₁₂H₂₅O₂P)₂(NO₃)₂]⁺: 751.2, 750.2, 752.2, found 751.2, 750.3, 752.2.

[Tb(4)₂(NO₃)₃] complex: FT-IR (ν , cm⁻¹): 1689 (C=O bound), 1121 (P=O); CHN analysis calculated (found) for [Tb(C₂₄H₅₀O₂P)₂(NO₃)₃(H₂O)₃]: C 33.40 (33.60), H 6.54 (6.21), N 4.87 (5.09); ESI-LRMS (M⁺, m/z) calcd of [Tb(C₁₂H₂₅O₂P)₂(NO₃)₂]⁺: 747.2, found 747.3.

Photophysical studies

All luminescence studies, unless otherwise noted, were carried out with a 1:2.25 ratio of lanthanide nitrate hydrate to ligand in HPLC grade CH₃CN. Solutions of complexes for absorption, emission and excitation spectra, as well as luminescence lifetime measurements, were prepared by combining appropriate volumes of metal and ligand 20 mM stock solutions to give an overall 2.0 mM concentration of Ln-ligand complex. The metal and ligand were massed into clean scintillation vials using an analytical balance. All photophysical measurements (other than the spectra acquired at 77K) were carried out at ambient temperature that was not regulated.

Quantum yields. Quantum yields were determined using the relative method.^{7, 27, 28} Quinine sulfate and fluorescein were used as the reference fluorophores, and the reported quantum yield values (Φ_u) were calculated by averaging the results from three trials with each fluorophore using Equation 1.

$$\Phi_u = \Phi_{std} \left(\frac{Grad_u}{Grad_{std}} \right) \left(\frac{\eta_u^2}{\eta_{std}^2} \right) \quad \text{Equation 1}$$

In Equation 1 Φ is the quantum yield, $Grad$ is the slope of the line of best fit from the dilution data, η is the refractive index of the solvent, u denotes the unknown compound, and std denotes the standard (or reference) fluorophore. The values used for each known quantity were taken from the literature as: $\Phi_{\text{quinine}} = 0.54$;²⁴ $\Phi_{\text{fluorescein}} = 0.79$;²⁷ $\eta_{\text{acetonitrile}} = 1.3441$; $\eta_{0.1 \text{ M NaOH}} = 1.3344$; $\eta_{0.1 \text{ M H}_2\text{SO}_4} = 1.3355$. A step-by-step procedure for how this data was measured, along with dilution curves for each trial, are provided in the Supplemental Information file.

Ligand singlet and triplet state energy. The triplet state energies of compounds **1-4** in acetonitrile were measured by recording emission spectra of the [Gd(**1-4**)_{2.25}(NO₃)₃] complexes at 77 K. Separate stock solutions of the ligand and metal nitrate were prepared and combined to give a solution of the 1:2.25 Ln-ligand complex at 2.0 mM complex concentration. The emission

spectra were recorded in both fluorescence ($\lambda_{\text{ex}} = 300$ nm; slit widths = 1.00-3.00 nm) and phosphorescence ($\lambda_{\text{ex}} = 300$ nm; slit widths = 1.00-2.00 nm; delay time = 0.05 ms; time per flash = 41.0 ms; sample window = 1.50 ms; flash count = 100) modes. The triplet state energy values were determined by deconvolution of the phosphorescence spectrum into its Gaussian components (OriginPro 2017). The peak corresponding to the highest energy vibration level obtained from the deconvolution was used to calculate each ligand's triplet state energy.²⁹

The excited singlet state energies of compounds **1-4** were determined from the room temperature UV/VIS absorption spectra of the 2.0 mM Gd(**1-4**)_{2.25}(NO₃)₃ complexes in acetonitrile. The value of the absorption edge^{30, 31} of each spectrum was determined using the method of Reddy and co-workers,³² and this was used to estimate the energy of the π - π^* singlet state.

Luminescence lifetimes. All lifetimes presented in this manuscript are results of fits of the data to a single exponential decay using Origin software. For some Ln(**1-4**)_{2.25}(NO₃)₃ complexes, the fitting of the decay data to a single exponential decay produced a curve which gave residuals that had shape (did not appear to be random). We attribute this to the fluxional nature of the Ln-ligand systems in solutions of acetonitrile, and that there are other decay processes in competition with metal-centered emission of light. In these instances, we attempted to fit the decay curve to a double exponential equation to try to capture the lifetimes of different complex stoichiometries or free metal in solution. Unfortunately, most of these attempts to fit the data to a double exponential decay were unsuccessful (did not converge). In one instance this fitting was successful (see data for the Eu(**3**)_{2.25}(NO₃)₃ complex in the SI file), but the resultant τ value was in good agreement to the τ obtained when the data was fit to a single exponential decay. As such, the data presented in the manuscript represent τ values where the decay curve was fit to a single exponential decay.

Computational studies

All models for this work were computed using the Gaussian 09 suite of programs, including use of Gaussview 5 to generate three-dimensional figures.^{33, 34} For the $[\text{Gd}(\mathbf{1})_2(\text{NO}_3)_3(\text{H}_2\text{O})]$ complex, an input structure was adapted from crystallographic data and imported into the gaussian input format. For the $[\text{Gd}(\mathbf{2-4})_2(\text{NO}_3)_3(\text{H}_2\text{O})]$ complexes, the atoms of the $[\text{Gd}(\mathbf{1})_2(\text{NO}_3)_3(\text{H}_2\text{O})]$ initial structure were used as a template and the drawing functionality in Gaussview was used to replace the appropriate -R groups to make a starter geometry for each structure. All structures were then optimized using the B3LYP density functional and the 6-311G(d) basis set for all atoms except gadolinium, for which the cep-121G effective core potential basis set was used. Geometries optimized with DFT were verified with frequency analysis at the same level of theory as the optimization to assure no imaginary vibrational frequencies. Each optimized structure was then further verified by scanning the potential energy surface, using Gaussian's modredundant functionality to check for lower energy structures by rotating around the more flexible single bonds. UV/Vis spectra predictions were also conducted at the same level of theory using time dependent DFT.

Results and Discussion

1. Synthesis of ligands and Ln-complexes. Ligands **1-4** were prepared using Arbuzov chemistry and are based on published methods (Figure 3).^{35, 36} Stirring the activated phosphines **5** or **6** with the desired α -bromoketone **7** or **8** in the absence of solvent gave the target β -ketophosphine oxides in reasonable yields. Arylphosphine oxides **1** and **2** required only trituration with diethyl ether for purification, while the alkylphosphine oxides **3** and **4** were purified using a combination of silica gel chromatography and Kugelrohr distillation. Compounds **1-4** were characterized by ^1H , ^{13}C , ^{31}P NMR, IR and HR-MS. The crystal structures of compounds **1** and **2** have been reported,^{37, 38} while compounds **3** and **4** were isolated as viscous liquids.

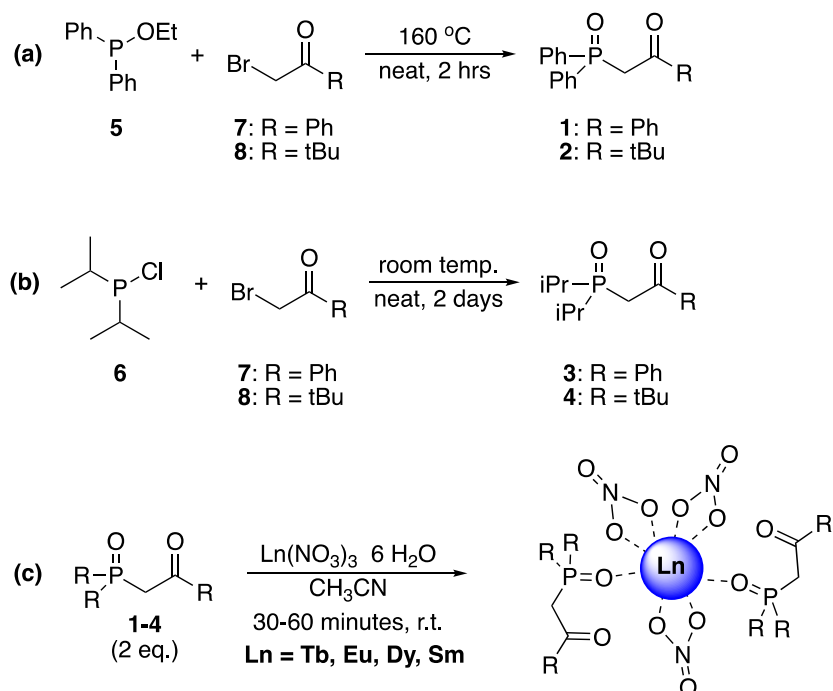


Figure 3. Synthesis of (a, b) ligands **1-4** and (c) the 1:2 Ln-ligand complexes.

Based on results from our previous work with compound **1**,¹⁴ we prepared 1:2 Ln³⁺-ligand complexes as solids for initial characterization purposes. We reported X-Ray crystal structures of ligand **1** complexed with a series of Ln(NO₃)₃ salts (Ln = Eu, Gd, Tb and Dy) and in each case the complex crystallized with a 1:2 ratio between the lanthanide metal and the ligand, even in the presence of excess ligand. Our luminescence work described below suggests that the ratio between lanthanide metal and ligand in solutions of acetonitrile is, on average, 1:2. Based on these results we prepared Ln-ligand complexes for each ligand **1-4** with the Ln(NO₃)₃ salts in a 1:2 ratio by mixing the two species in acetonitrile at room temperature. The complexes were purified by trituration with diethyl ether to give fine powders. Analysis of the complexes for CHN composition revealed that when prepared using this method each complex contains 1-3 solvent water molecules which are likely remnants from the hydrated Ln(NO₃)₃ starting salts. Each 1:2 Ln³⁺-ligand complex was also characterized by low-resolution mass spectrometry (LR ESI-MS) and IR spectroscopy, and the Sm³⁺ complexes were characterized by ¹H, ¹³C and ³¹P NMR spectroscopy.

2. Characterization of Ln-ligand complexes by IR spectroscopy and low-resolution mass spectrometry. The 1:2 Ln(NO₃)₃-ligand complexes were first characterized by IR spectroscopy as solids as well as by LR-MS as dilute solutions in acetonitrile. For the IR analysis, the frequency of the stretches for the C=O and P=O bonds are given in Table 1. For each ligand-Ln(NO₃)₃ combination, the stretches corresponding to both the C=O and P=O bonds of the ligand moved to lower wavenumbers ($\Delta\nu$ 3-30 and 30-70 cm⁻¹, respectively) upon metal complexation. This indicates a weakening of these bonds as they donate electron density to form the Ln³⁺-O bond in the complex. For complexes containing ligands **2** and **3**, stretches were also observed at the same frequency as the C=O bond in the free ligand.

Inspection of the magnitude of the changes in the bond stretch frequency reveals some information about the nature of bonding between each ligand and the Ln³⁺ metals. The first feature that stands out is the larger change in bond frequency ($\Delta\nu$) observed for the P=O group vs. the C=O group. This is an indication that the interaction between the Ln³⁺ metal and the P=O group is stronger than that with the C=O group in the solid state. This is consistent with the idea that a P=O bond is more polarized than a C=O bond, which should make it a stronger donor to a Ln³⁺-O bond.

The second feature worth pointing out is that the $\Delta\nu$ for the P=O bonds of ligands **3** and **4** is approximately double that seen for ligands **1** and **2**. The substituents of ligands **3** and **4** are alkyl groups, which are electron donating (versus the electron withdrawing phenyl rings of ligands **1** and **2**). The alkyl groups create a more electron-rich phosphine oxide in **3** and **4**, which should form a stronger interaction with a Ln³⁺ metal. This stronger interaction is evidenced by the larger $\Delta\nu$ values observed in the IR spectra of these complexes. This pattern is also observed when comparing the carbonyl stretches of ligands **1** and **2**. The C=O $\Delta\nu$ is much larger for the alkyl carbonyl **2** vs. the aryl carbonyl **1**.

The last feature of the IR spectra that we found interesting was the magnitude of the $\Delta\nu$ values of the phosphine oxide and carbonyl bonds. It appears that, based purely on the magnitude of the $\Delta\nu$ values of the phosphine oxide and carbonyl bonds, ligand **3** interacts with the Ln³⁺ metals the strongest in the solid state. The relatively electron poor aryl carbonyl group of **3** shows the largest $\Delta\nu$ values of the series, even though it bears an electron withdrawing aryl group. We attribute this to the stronger bond between the phosphine oxide and the Ln³⁺ rather than to a property of the carbonyl bond.

The stretches corresponding to the nitrate groups were also analyzed to determine the nature of the Ln-nitrate interaction in the complexes in the solid state. Following the work of previous groups,³⁹⁻⁴² stretches corresponding to the $\nu(\text{N}=\text{O})$, $\nu_a(\text{NO}_2)$ and $\nu_s(\text{NO}_2)$ bonds were found in the IR spectra of the complexes around 1450, 1290 and 1030 cm^{-1} respectively. The relatively large difference between the energies of the $\nu(\text{N}=\text{O})$ and $\nu_a(\text{NO}_2)$ absorption bands ($\Delta\nu = 164\text{-}189 \text{ cm}^{-1}$) is indicative of the presence of inner-sphere, bidentate nitrate groups. This was supported by the observation of a stretch at 815 cm^{-1} in the IR spectrum of each complex which is typical of a bidentate nitrate group. Lastly, very small absorbances were seen that could be attributed to the presence of an outer-sphere, anionic nitrate ($\sim 1390 \text{ cm}^{-1}$). Based on this analysis we propose that the inner sphere of the Ln^{3+} metal in these complexes contains two ligands, bonded in a mixture of monodentate binding through the P=O group and bidentate binding with both the P=O and C=O groups, along with 2-3 bidentate nitrate groups.

Table 1. FT-IR absorption bands (cm^{-1}) for ligands **1-4** and their complexes with $\text{Ln}(\text{NO}_3)_3$ ($\text{Ln} = \text{Tb}, \text{Eu}, \text{Sm}, \text{Dy}$) as solids. The $\Delta\nu$ column under the carbonyl and phosphine oxide headings is the difference in peak location for that functional group between the free and complexed ligands. Specific assignments for the nitrate absorption bands are given in a table in the Supplementary Information file.

Ligand or Complex	carbonyl stretch		phosphine oxide stretch		Coordinated nitrate $\Delta\nu$ $\nu(\text{N}=\text{O})$ and $\nu_a(\text{NO}_2)$
	$\nu(\text{C}=\text{O})$	$\Delta\nu$	$\nu(\text{P}=\text{O})$	$\Delta\nu$	
ligand 1	1680	---	1179	---	---
$\text{Sm}(\mathbf{1})_2(\text{NO}_3)_3$	1675	5	1154	25	173
$\text{Eu}(\mathbf{1})_2(\text{NO}_3)_3$	1673	7	1154	25	177
$\text{Tb}(\mathbf{1})_2(\text{NO}_3)_3$	1674	6	1154	25	164
$\text{Dy}(\mathbf{1})_2(\text{NO}_3)_3$	1674	6	1155	24	180
ligand 2	1699	---	1187	---	---
$\text{Sm}(\mathbf{2})_2(\text{NO}_3)_3$	1684	15	1156	31	182
$\text{Eu}(\mathbf{2})_2(\text{NO}_3)_3$	1671	28	1154	33	183
$\text{Tb}(\mathbf{2})_2(\text{NO}_3)_3$	1671	28	1154	33	187
$\text{Dy}(\mathbf{2})_2(\text{NO}_3)_3$	1670	29	1154	33	189
ligand 3	1669	---	1178	---	---
$\text{Sm}(\mathbf{3})_2(\text{NO}_3)_3$	1640	29	1107	71	174
$\text{Eu}(\mathbf{3})_2(\text{NO}_3)_3$	1639	30	1108	70	180
$\text{Tb}(\mathbf{3})_2(\text{NO}_3)_3$	1637	32	1108	70	179
$\text{Dy}(\mathbf{3})_2(\text{NO}_3)_3$	1638	31	1109	69	178
ligand 4	1698	---	1172	---	---
$\text{Sm}(\mathbf{4})_2(\text{NO}_3)_3$	1690	8	1123	49	185
$\text{Eu}(\mathbf{4})_2(\text{NO}_3)_3$	1691	7	1117	55	186
$\text{Tb}(\mathbf{4})_2(\text{NO}_3)_3$	1689	9	1121	51	183
$\text{Dy}(\mathbf{4})_2(\text{NO}_3)_3$	1691	7	1116	56	183

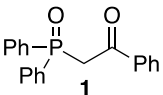
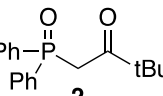
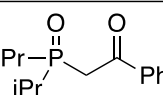
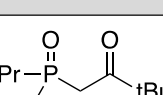
The stoichiometry of the $[\text{Ln}(\mathbf{1-4})_2(\text{NO}_3)_3]$ complexes in solution was then investigated by low resolution mass spectrometry (LR-MS) with electrospray ionization. The solid complexes were injected as dilute solutions in acetonitrile and gave MS spectra showing peaks corresponding to 1:2 Ln-ligand complexes that were ionized by the loss of either one or two nitrate groups.

3. Characterization of the Sm^{3+} complexes in solution using NMR.

The solid $[\text{Sm}(\mathbf{1-4})_2(\text{NO}_3)_3]$ complexes were characterized in solutions of CD_3CN using ^1H , ^{13}C and ^{31}P NMR spectroscopy (Table 2). For all four $\text{Sm}(\text{NO}_3)_3$ -ligand complexes, the signal corresponding to the hydrogen atoms of the methylene group of the ligand shifted downfield relative to the ligand alone with $\Delta\delta$ values ranging from 0.45-0.86 ppm. A similar trend was observed in the ^{31}P NMR spectra for the resonance corresponding to the phosphorus atom of the phosphine oxide group, with $\Delta\delta$ values ranging from 11.0-16.7 ppm. Interestingly, analysis of the ^{13}C NMR spectra showed that the signal corresponding to the carbonyl carbon shifted downfield slightly upon complexation with $\text{Sm}(\text{NO}_3)_3$ ($\Delta\delta = 1.1$ - 3.7 ppm), while the resonance for the carbon atom of the methylene group shifted upfield ($\Delta\delta = -3.8$ to -0.9 ppm). Regardless of the nucleus observed by NMR, all spectra showed one set of signals, rather than two separate sets of signals that could be attributed to both free and bound ligand. We take these results to mean that, in solutions of acetonitrile, the ligand undergoes an on-off exchange process with the metal that is fast on the ^1H , ^{31}P and ^{13}C NMR timescales. Due to the significant change in the chemical shift observed for the phosphine oxide phosphorus resonance we believe that this group is interacting with the metal in solution most of the time. The relatively small change in chemical shift in the resonance for the carbonyl carbon, as well as the upfield shift for the resonance of the methylene carbon, suggests that the carbonyl group is exchanging between bound and unbound conformations in solution. These hypotheses correlate with IR (*vide supra*) and single crystal X-ray diffraction data for complexes of ligand **1**^{14, 43} that show the presence of both a bound and unbound C=O group in these metal-ligand complexes in the solid state.

Further inspection of the ^{31}P NMR data reveals that the compound with the largest $\Delta\delta$ upon complexation to Sm^{3+} is ligand **3**, followed by ligand **4** and then **1** and **2**. A similar trend is seen in the ^1H NMR data. We propose that ligands **3** and **4** spend more time bonded to the metal in solution versus ligands **1** and **2**, and this is the reason for the larger observed $\Delta\delta$ values. Ligands **3** and **4** share the common feature of bearing isopropyl groups on the phosphorus atom rather than phenyl rings, and we again suggest that the more electron donating alkyl groups have created a more electron rich phosphine oxide group which is, in turn, a stronger ligand for the Sm^{3+} metal.

Table 2. Chemical shifts of diagnostic resonances (ppm) for ligands **1-4** and their complexes with Sm(NO₃)₃ in CD₃CN.

	¹ H NMR	¹³ C NMR		³¹ P NMR
	-CH ₂ -	C=O	-CH ₂ -	P=O
	4.28	193.5	42.5	26.4
Sm(1) ₂ (NO ₃) ₃	4.70	195.2	39.1	37.7
Δδ	0.43	1.7	-3.4	11.7
	3.80	208.4	39.0	26.5
Sm(2) ₂ (NO ₃) ₃	4.31	210.9	38.1	37.5
Δδ	0.51	2.5	-0.9	11.0
	3.53	195.4	36.7	54.3
Sm(3) ₂ (NO ₃) ₃	4.30	197.3	32.9	71.0
Δδ	0.77	1.9	-3.8	16.7
	3.09	210.3	33.6	55.1
Sm(4) ₂ (NO ₃) ₃	3.95	214.0	31.8	70.0
Δδ	0.86	3.7	-1.8	14.9

3. Luminescence studies.

Our first set of experiments in this area involved identifying the solution speciation between Ln(NO₃)₃ and ligands **1-4** that would give the most intense luminescence emission. We carried out luminescence titrations in acetonitrile with varying equivalents of ligands **1** and **2** with Eu(NO₃)₃ and found that solutions with 2.25 equivalents of ligand displayed the most intense emission. This agrees well with our X-Ray crystallographic results with ligand **1** where 1:2 Ln(NO₃)₃-ligand complexes were obtained in the solid state even in the presence of three equivalents of ligand.¹⁴ We attribute the increase in fluorescence intensity with more than two equivalents of ligand to the nature of these dynamic Ln(NO₃)₃-ligand complexes in solution. We

suggest that while a 1:2 Ln(NO₃)₃-ligand ratio represents the maximum number of these ligands that will bind to the inner-coordination sphere of the metal, there is a fast on-off exchange process occurring and the presence of a slight excess of ligand ensures complete complexation of the metal. Using these results we chose to carry out all luminescence experiments with 1:2.25 Ln(NO₃)₃-ligand ratio.

Absorption, excitation and corrected emission spectra are shown for each 1:2.25 Ln(NO₃)₃-**(1-4)** complex in Figure 4. These spectra were acquired in solutions of acetonitrile where the concentration of the metal was 2.0 mM. For the excitation spectra, emission was monitored at the most intense peak for each Ln³⁺ metal: Tb³⁺ = 543 nm, Eu³⁺ = 616 nm, Dy³⁺ = 573 nm, Sm³⁺ = 642 nm. For the emission spectra, the excitation wavelength was set at 300 nm for each complex based on the λ_{max} values from the complexes' UV-Vis spectra. In the interest of space, we have plotted one graph per ligand in this figure; separate plots for each Ln-ligand complex are shown in the Supplemental Information.

To the naked eye the Tb- and Eu(**1-4**)_{2.25}(NO₃)₃ complexes displayed the most intense emission and show characteristic bands^{24, 44} that are nearly identical for each ligand. The Tb³⁺ complexes show large peaks at 488 and 543 nm, with less intense peaks at 585 and 623 nm. These peaks correspond to transitions between the ⁵D₄ emissive state and the ⁷F_J manifold (*J* = 6, 5, 4, 3, respectively). The emission spectra of the Eu³⁺ complexes show peaks at 593 and 615 nm (⁵D₀ → ⁷F_J transitions, *J* = 1, 2), where the peak at 615 nm is much more intense than the peak at 593 nm. Peaks for the ⁵D₀ → ⁷F_J transitions where *J* = 0, 3 and 4 are also observed, although they are much less intense.

A closer look at the excitation and emission spectra of the complexes with ligands **2** and **4** reveals some interesting features. First, ligand emission is seen as a low-intensity, broad peak centered around 400 nm. This is some indication that the excited states of these ligands are not as efficient at populating the excited state of the metals as their counterparts **1** and **3**. Second, the excitation spectra show small *f-f* transition peaks for each Ln³⁺ complex (see spectra in Supplemental Information file). This is an indication that direct excitation of the metal is a process that is competing with excitation of the ligand.

Emission of the Dy- and Sm(**1-4**)_{2.25}(NO₃)₃ complexes was much dimmer than their Tb³⁺ and Eu³⁺ counterparts, but they did show characteristic bands in the luminescence spectra for each complex. The peaks corresponding to metal-centered emission in the luminescence spectra of the

Dy³⁺ complexes were nearly identical regardless of the ligand, with bands at 482 and 574 nm (⁴F_{9/2} → ⁶H_J transitions, *J* = 15/2 and 13/2). For the Dy³⁺-complexes with ligands **2** and **4**, a broad signal was observed that is centered around 400 nm which we assign to ligand emission. This is some indication that the excited states of ligands **2** and **4** are not as efficient at populating the accepting state of the Dy³⁺ ion as ligands **1** and **3**.

The emission spectra of the Sm(**1-4**)_{2.25}(NO₃)₃ complexes also show characteristic peaks for metal-centered emission. All four ligands are capable of sensitizing emissions at 562, 596 and 643 nm (⁴G_{5/2} → ⁶H_J transitions, *J* = 5/2, 7/2 and 9/2). The emission spectra of the Sm³⁺ complexes with ligands **1** and **3** show no ligand emission, while the complexes of ligands **2** and **4** show a significant amount of ligand emission. For the Sm³⁺ complexes with ligands **2** and **4**, when the emission spectra were acquired at 77K a decrease in the intensity of the ligand emission was observed (spectra shown in Supplemental Information). This is an indication that back transfer from the metal along with radiative decay from the ligand are processes that compete with energy transfer to the Sm³⁺ metal.

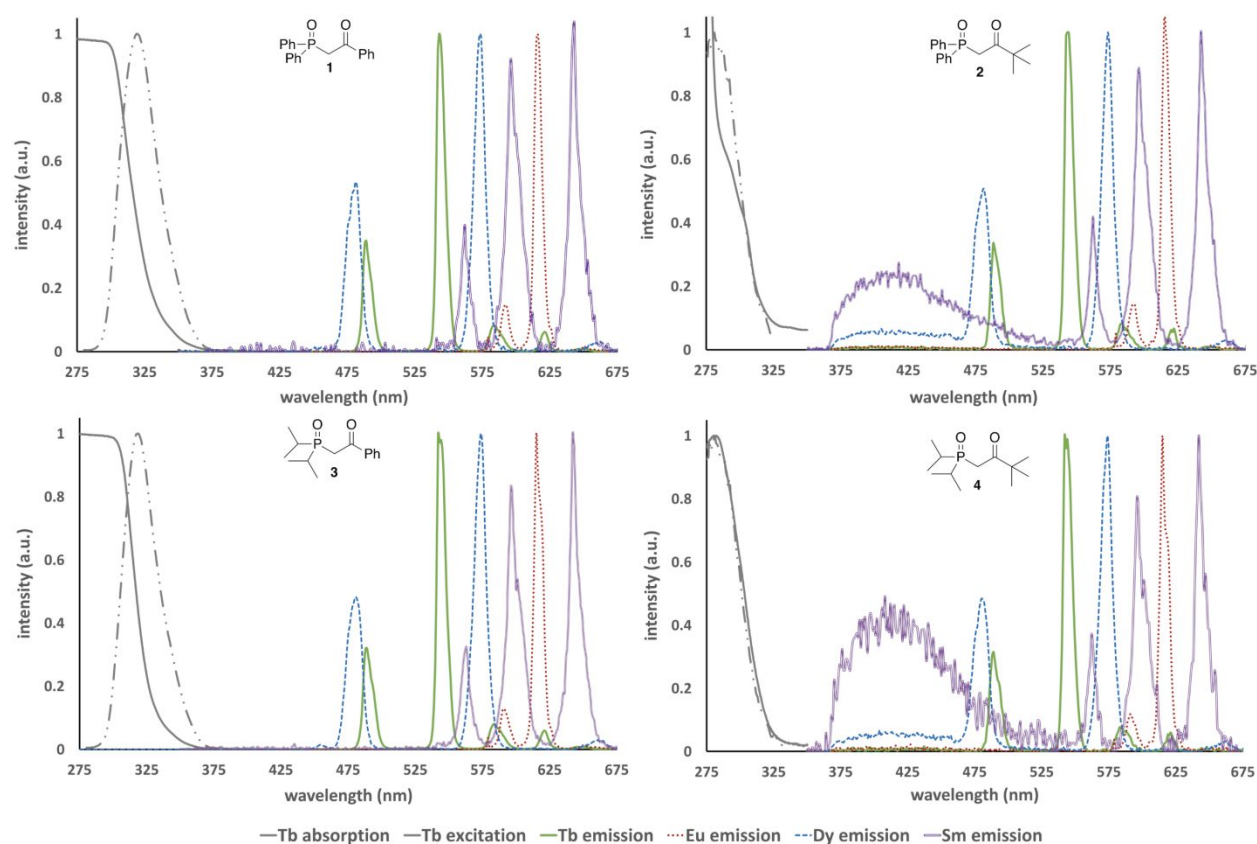


Figure 4. Absorption, excitation and corrected emission spectra for the Ln(**1-4**)_{2.5}(NO₃)₃ complexes in acetonitrile (2.0 mM complex concentration). The structure of the ligand is shown at the top of each set of spectra. The absorption and excitation spectra were very similar for each set of ligand complexes, so only the spectra for the Tb³⁺ complexes are shown here for clarity. All absorption and excitation spectra are shown in the supplemental information file. Key: Tb³⁺ absorption: solid grey; Tb³⁺ excitation: dash/dotted grey; Tb³⁺ emission: solid green; Eu³⁺ emission: dotted red; Dy³⁺ emission: dashed blue; Sm³⁺ emission: open purple. The intensities of each spectrum have been normalized for ease of comparison. For excitation and emission spectra, both entrance and exit slit widths were set at 1.0 nm for the Tb³⁺ and Eu³⁺ complexes, and 1.5 nm for the Dy³⁺ and Sm³⁺ complexes.

Additional insight into the solution structure of the complexes can be gained by looking closely at the emission spectra of each of the Eu³⁺ complexes. The emission spectrum of the Eu(**1**)_{2.5}(NO₃)₃ complex is shown in Figure 5, where the peaks corresponding to each of the ⁵D₀ → ⁷F_J transitions (*J* = 0-4) have been labeled. As expected,^{45, 46} the hypersensitive *J* = 2 transition is the most intense of all of the peaks in this spectrum and indicates that the Eu³⁺ complex has relatively low symmetry. A second indication of this low-symmetry environment is the peak at 580 nm that corresponds to the ⁵D₀ → ⁷F₀ transition. When the emission spectra of the Eu(**2-4**)_{2.5}(NO₃)₃ complexes are inspected, similar peak shapes and intensities are observed for all transitions from one spectrum to another. This is an indication that each of the Eu³⁺-ligand complexes has a similar coordination geometry and stoichiometry in solutions of acetonitrile.

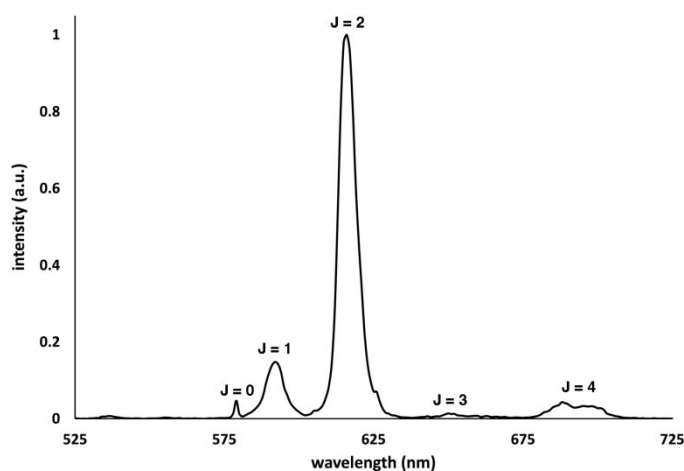


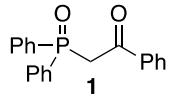
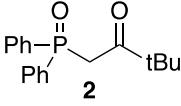
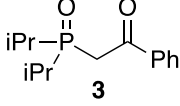
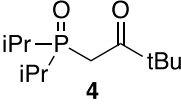
Figure 5. Corrected emission spectrum of the $\text{Eu}(\mathbf{1})_{2.25}(\text{NO}_3)_3$ complex in acetonitrile ($[\text{Eu}] = 2.0$ mM; excitation wavelength = 300 nm; entrance and exit slit widths = 1.0 nm). Each peak is labeled as the J value for the corresponding ${}^5\text{D}_0 \rightarrow {}^7\text{F}_J$ transition.

Luminescence lifetime and quantum yield measurements. Luminescence lifetimes of each ligand **1-4** with the $\text{Ln}(\text{NO}_3)_3$ salts in acetonitrile are listed in Table 3 ($\text{Ln} = \text{Tb}, \text{Eu}, \text{Sm}$), along with the quantum yield values for the Tb^{3+} and Eu^{3+} complexes. We attempted to measure the lifetime values for the Dy^{3+} complexes under these conditions, but the experiments suffered from poor solubility of the complexes in acetonitrile and, hence, numbers that were not reproducible. Our decision to measure quantum yield values for only the Tb^{3+} and Eu^{3+} complexes was simply because their emission was the most intense.

The lifetime and quantum yield experiments were carried out with 2.25 equivalents of ligand to metal at a $\text{Ln}(\text{NO}_3)_3$ -ligand complex concentration of 2.0 mM. The lifetimes in Table 3 are the results of fits of the data to a single exponential decay and are averages of three trials (decay curves and fit statistics are given in the Supplemental Information file). Quantum yield values were determined using the dilution method with quinine sulfate and fluorescein as standards.^{24, 27}

The luminescence lifetimes for complexes with ligand **1** fall in the range of expected values for each metal. The quantum yields for the Tb^{3+} and Eu^{3+} complexes are also reasonable at 19.2 and 8.7%, respectively. Lifetimes for complexes of ligand **2**, where the aryl carbonyl has been replaced with an alkyl carbonyl group, are slightly longer for each metal, however the quantum yields for both the Tb^{3+} and Eu^{3+} complexes drop to 7.6 and 5.5%. For complexes of ligand **3** the lifetime values are notably shorter for each metal, yet the quantum yields are the highest of this study at 29.8 and 11%. Lastly, the lifetime values for complexes of ligand **4** are the longest of any ligand, yet the quantum yields are the lowest measured here at 1.8 (Tb^{3+}) and 1.2% (Eu^{3+}).

Table 3. Values for various photophysical parameters of the $[\text{Ln}(\mathbf{1-4})_{2.25}(\text{NO}_3)_3]$ complexes in acetonitrile (2.0 mM metal concentration, $\lambda_{\text{ex}} = 300$ nm). The lifetime and quantum yield values represent the average with standard error from three trials. Lifetime measurements were monitored at these wavelengths: 543 nm (Tb^{3+}), 616 nm (Eu^{3+}), 641 nm (Sm^{3+}).

ligand					
lifetimes (τ_{obs} , ms)	Sm	0.0386 ± 0.0002	0.040 ± 0.002	0.022 ± 0.002	0.045 ± 0.002
	Eu	0.9333 ± 0.0009	0.99 ± 0.01	0.717 ± 0.004	1.402 ± 0.004
	Tb	1.571 ± 0.001	1.80 ± 0.02	1.367 ± 0.002	1.86 ± 0.02
quantum yields (%)	Eu	8.7 ± 0.2	5.5 ± 0.3	11 ± 1	1.2 ± 0.2
	Tb	19.2 ± 0.7	7.6 ± 0.5	29.8 ± 0.9	1.8 ± 0.3
τ_{rad} (ms)		3.46	3.41	3.24	3.24
k_{rad} (s^{-1})		289	293	309	309
k_{nr} (s^{-1})		782	717	1090	405
$\Phi_{\text{f-f}}$ (%)		27	29	22	43
singlet state energy (calculated) (cm^{-1})		29,900 (26,200)	31,300 (30,000)	30,500 (26,600)	31,400 (30,600)
triplet state energy (calculated) (cm^{-1})		24,400 (24,600)	22,900 (27,600)	24,600 (24,900)	23,600 (23,800)
ΔE ($^1\text{S} - ^3\text{T}$) (cm^{-1})		5,500	8,400	5,900	7,800

Based on this data, it appears that compounds **1** and **3**, which bear an aryl carbonyl group, are the best ligands to sensitize metal-centered emission resulting in the highest quantum yield values for this series. However, compounds **2** and **4**, which bear an alkyl (*t*-butyl) carbonyl group, are the best ligands to protect the excited state of the metal resulting in the longest lifetime values. For each of the complexes described here, we propose that metal-complexation occurs primarily through a bond between the Ln(III) metal and the phosphine oxide group, as evidenced by prior X-Ray diffraction data^{14, 43, 47, 48} as well as the IR and NMR data discussed

above. In this coordination geometry, the substituent on the carbonyl group will be present in the second coordination sphere of the metal. In the case of complexes with ligands **2** and **4**, this substituent is the bulky and hydrophobic *t*-butyl group. We propose that due to the steric bulk of this substituent, the access of quenchers such as adventitious water and CH₃CN molecules to the metal is restricted more so than when a phenyl group is present. This argument could explain the longer lifetimes observed for complexes with ligands **2** and **4**.

Lastly, using the emission spectra of the Eu³⁺ complexes we estimated the radiative and non-radiative rate constants (k_r and k_{nr}), the 4*f*-4*f* emission quantum yield (Φ_{f-f}) and the radiative emission lifetime (τ_{rad}) using Equations 2-4 shown below. The radiative emission lifetime is defined as the ideal emission lifetime without nonradiative processes. In these equations τ_{obs} is the observed emission lifetime, $A_{MD,0}$ is the spontaneous emission probability for the ⁵D₀ → ⁷F₁ transition in vacuo (14.65 s⁻¹),⁴⁹ n is the refractive index of acetonitrile ($n = 1.3441$), and I_{tot}/I_{MD} is the ratio of the total area of the corrected Eu³⁺ emission spectrum to the area of the ⁵D₀ → ⁷F₁ transition.^{46, 50} The values for these radiative parameters are listed in Table 3.

$$k_r = \frac{1}{\tau_{rad}} = (A_{MD,0})(n^3) \frac{I_{tot}}{I_{MD}} \quad \text{Equation 2}$$

$$\Phi_{f-f} = \frac{k_r}{k_r + k_{nr}} = \frac{\tau_{obs}}{\tau_{rad}} \quad \text{Equation 3}$$

$$k_{nr} = \frac{1}{\tau_{obs}} - \frac{1}{\tau_{rad}} \quad \text{Equation 4}$$

For the Eu³⁺ complexes of each ligand **1-4** the value for the radiative (ideal) emission lifetime (τ_{rad}) is similar across the series and ranges from 3.24 to 3.46 ms. These lifetime values correspond to radiative rate constants (k_r) ranging from 289 to 309 s⁻¹. The similarity in these parameters is another indication that the overall geometry (e.g. stoichiometry, point group) of the complexes is similar in solutions of acetonitrile. The values of the non-radiative rate constant (k_{nr}), however, differ slightly between the ligands. Complexes of ligands **1** and **2** have similar k_{nr} values of 782 and 717 s⁻¹, respectively. This makes sense as the inner coordination sphere of the complexes is composed of the phosphine oxide group which, in the case of ligands **1** and **2**, bears the same phenyl ring substituent. The value of k_{nr} is the largest for complexes of ligand **3** (1090 s⁻¹) while it is the smallest for complexes of ligand **4** (405 s⁻¹). The rate of non-radiative decay

could be one contributor to the measured overall quantum yield values for these complexes. For complexes of ligand **3** we see the highest overall quantum yield of the series, which agrees with a set of relaxation processes where those involving non-radiative decay are longer. Conversely, complexes of ligand **4** have the smallest rate constant for non-radiative decay processes and these complexes also have the lowest overall quantum yield values measured here.

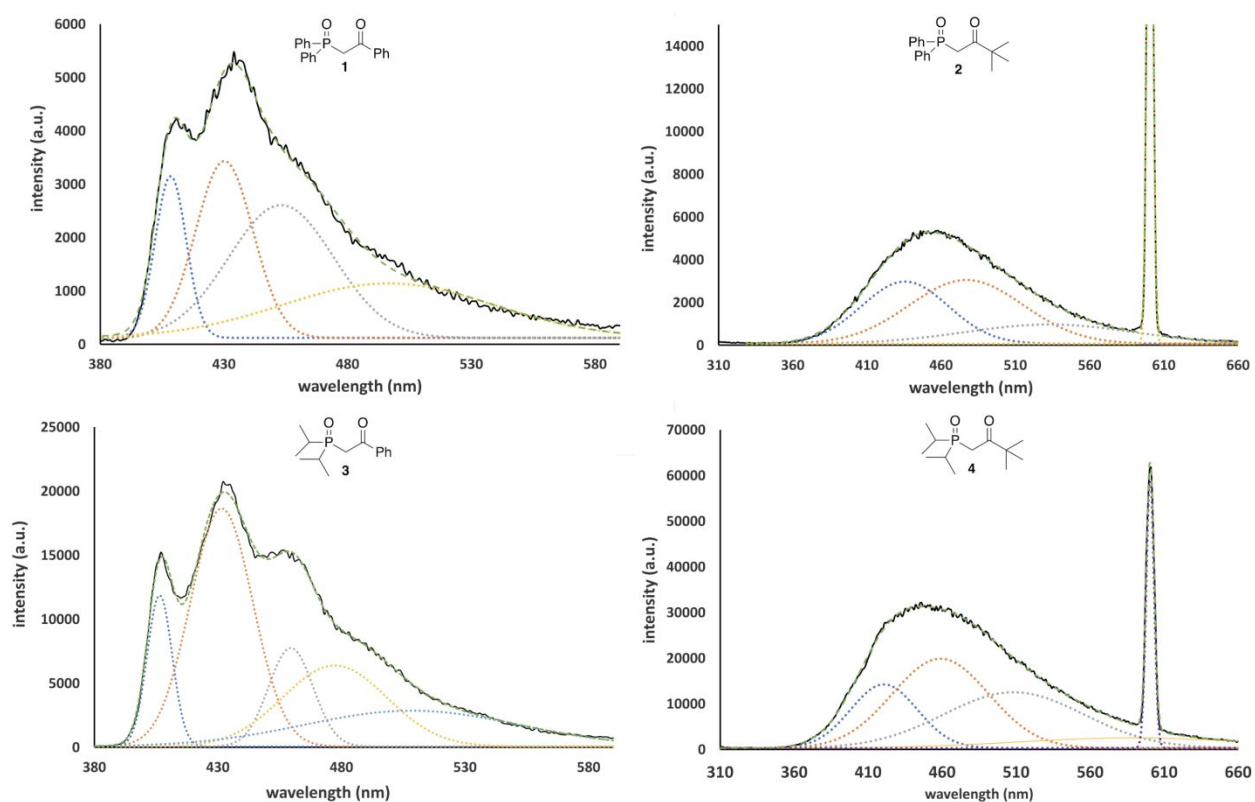


Figure 6. Deconvolution of 77K phosphorescence spectra ($\lambda_{\text{ex}} = 300 \text{ nm}$) of the $[\text{Gd}(\mathbf{1}-\mathbf{4})_{2.25}(\text{NO}_3)_3]$ complexes in CH_3CN . The structure of the ligand is shown at the top of each spectrum. The peaks at 600 nm are at double the excitation wavelength and are an artifact. Slit widths (excitation, emission): **1** = 1,1 nm; **2** = 3,1.5 nm; **3** = 1,1 nm; **4** = 1,2 nm. Key: phosphorescence spectrum: black solid line; fit peaks: colored dotted lines; calculated sum of fit peaks: green dashed line.

Determination of ligand triplet state energy. To help explain the trend in quantum yield values we turned our efforts toward the determination of the energy of the singlet and triplet excited

states of each ligand. The $[\text{Gd}(\mathbf{1-4})_{2.25}(\text{NO}_3)_3]$ complexes were prepared in acetonitrile (2.0 mM Gd^{3+} concentration) and cooled to 77K. Emission spectra in both fluorescence and phosphorescence (delay time = 0.05 ms) mode of the complexes was obtained at this temperature, and those acquired in phosphorescence mode are shown in Figure 6. The phosphorescence spectra were then deconvoluted into their vibrational components using OriginPro software. In this deconvolution, the highest energy (lowest wavelength) band is considered to be the energy state that is mostly responsible for populating the metal.²⁵ Analysis of the fluorescence spectra in a similar way resulted in singlet state energies that were quite close to the triplet state energies (ΔE 1000-2000 cm^{-1}), and we suspect that we were not capturing emission from the singlet state of the ligand with this technique since the singlet state of Ln-ligand complexes can be short lived.²⁵

We then turned to the room temperature UV/VIS absorption spectra of the Gd^{3+} complexes, and used the value of the absorption edge^{30,31} to estimate the energy of the $\pi\text{-}\pi^*$ singlet state as described by Reddy and co-workers.³² The 77K fluorescence spectra and room temperature UV/VIS absorption spectra of the $[\text{Gd}(\mathbf{1-4})_{2.25}(\text{NO}_3)_3]$ complexes are shown in the Supplemental Information file. The values of each ligand's singlet and triplet state energies are given in Table 3.

The energies of each ligand's excited triplet state are fairly consistent across the series, with ligands **1** and **3** having slightly higher values at 24,400 and 24,600 cm^{-1} compared to those of ligands **2** and **4** at 22,900 and 23,600 cm^{-1} . The values of these ligands' triplet states are close to the energy of the accepting metal f excited states at 20,430 cm^{-1} for Tb^{3+} and 19,020 and 17,250 cm^{-1} for Eu^{3+} . It is a general guideline that the ideal size of the energy gap between the ligand's triplet state and the metal's accepting f excited state is $\sim 2000\text{-}4000$ cm^{-1} ,²⁵ and all four ligands are close to this value. The energies of the singlet states are also fairly consistent from ligand to ligand, but in this case ligands **2** and **4** have higher lying singlet states when compared to **1** and **3**. The result of this is that the difference in energy between the triplet and singlet states is larger for ligands **2** and **4**.

In the case of the two most efficient ligands in this process, ligands **1** and **3**, we see that they have closely lying singlet and triplet states ($\Delta E = 5,500$ and $5,900$ cm^{-1} , respectively), so intersystem crossing (ISC) should be favorable. We propose that one reason the quantum yield of ligand **3** is higher than that of ligand **1** is due to the electron donating alkyl substituent present on

the phosphine oxide group. The ^1H and ^{31}P NMR data discussed above suggests that ligand **3** spends more time complexed to the metal in solution, which should result in more opportunities for the ligand to transfer energy to the metal versus access other decay pathways.

In the case of the less efficient ligands **2** and **4**, we see a larger gap between the excited singlet and triplet states ($\Delta E = 8,400$ and $7,800\text{ cm}^{-1}$, respectively) which is an indication that intersystem crossing (ISC) may be less favored in these two systems in lieu of other forms of ligand relaxation. Inspection of the emission spectra from the Tb^{3+} - and Eu^{3+} -complexes with ligands **2** and **4** also show some emission from the free ligand, albeit small. This is one piece of evidence that some energy that has been absorbed by the ligand is not being transferred to the metal, which would decrease the quantum yield value.

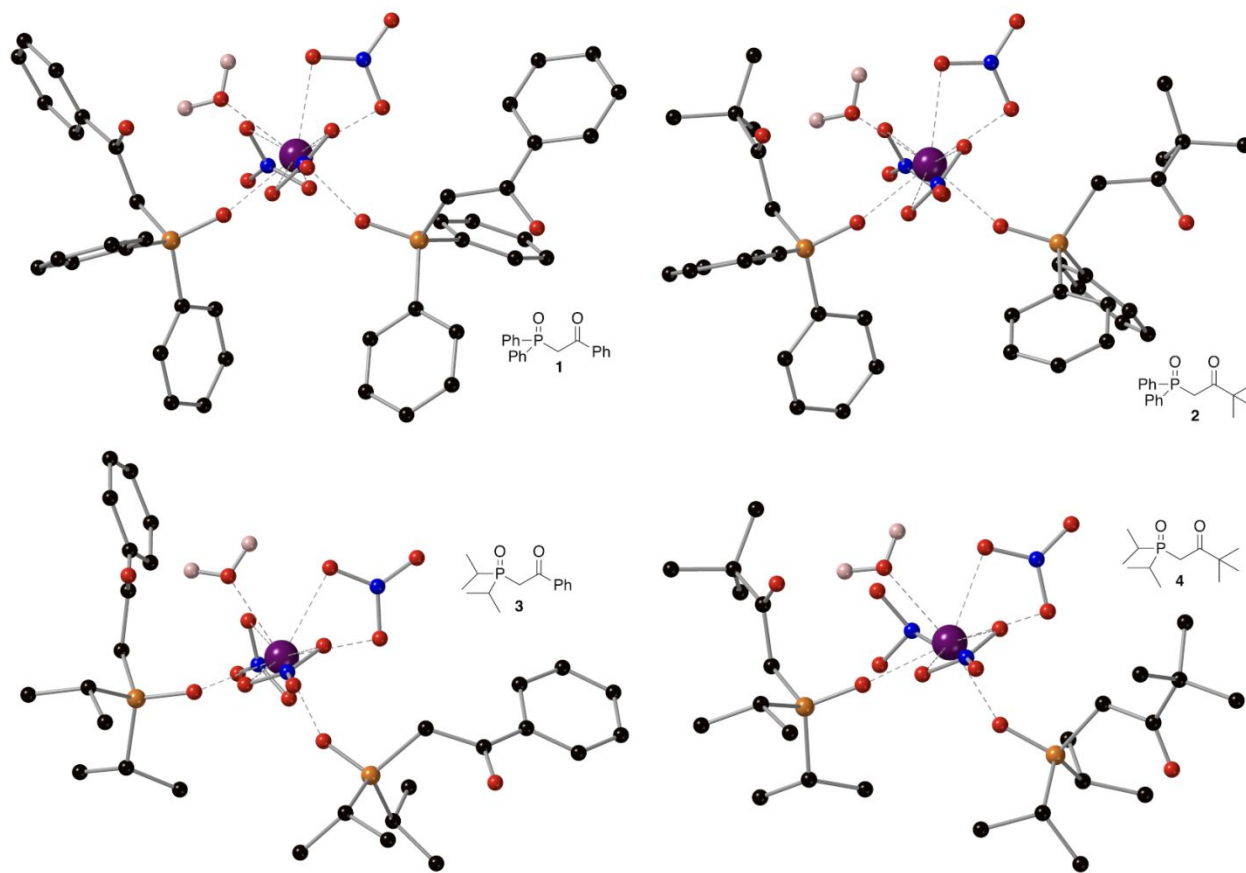


Figure 7. Geometry optimized structures of the triplet excited state of the $\text{Gd}(\mathbf{1-4})_2(\text{NO}_3)_3(\text{H}_2\text{O})$ complexes using a ball and stick model with standard CPK colors (Gd = purple). The structure of the ligand is shown near each complex, and only the hydrogen atoms of the water molecule are shown for clarity.

To support these experimental numbers, we carried out DFT calculations using Gaussian 09³³ to predict the values of the excited states. Starting with the coordinates from the single crystal X-Ray structure of the $[\text{Gd}(\mathbf{1})_2(\text{NO}_3)_3(\text{H}_2\text{O})]$ complex,¹⁴ we modified the appropriate substituents on the ligands using GaussView³⁴ to build structures of the $\text{Gd}(\text{NO}_3)_3$ complexes of ligands **2**, **3** and **4**. The geometry of each complex was then optimized using the B3LYP density functional and a combination of the 6-311(d) (for C, H, N, O, P) and cep-121G (for Gd) basis sets. Calculation of the singlet state energies was done using time dependent DFT calculations, and the triplet state energies were determined by subtracting the calculated energy of the ground state from the calculated energy of the triplet state. Figure 7 shows the geometry of the complexes in the excited triplet state, while the structures for the singlet states are shown in the Supplemental Information file.

The calculated numbers for the triplet state energies of ligands **1**, **3** and **4** agree quite well with our experimental numbers. Unfortunately, the calculated value for the energy of the triplet state of compound **2** does not agree with the experimental value. At this point we do not have an explanation for this discrepancy, but based on the consistency of the experimental values for each ligand we are confident that the experimental value for compound **2** is correct. The calculated singlet state energies are within 10% of the experimental values and support the idea that the singlet states of ligands **2** and **4** are higher in energy than those of ligands **1** and **3**.

Summary and Outlook

This paper described the synthesis of four β -carbonylphosphine oxide ligands along with their complexes with four $\text{Ln}(\text{NO}_3)_3$ salts ($\text{Ln} = \text{Sm}, \text{Eu}, \text{Tb}, \text{Dy}$). IR and NMR data suggest that Ln^{3+} complexation occurs primarily through the phosphine oxide group of the ligand, with minor bonding through the carbonyl group. This data, along with quantum yield data, also suggests that the ligands with the more electron rich phosphine oxide groups bind more strongly to the Ln^{3+} metals, while the ligands with bulky substituents on the carbonyl group may have a protective effect on the excited state of the metal.

The applications of this work can be found in the design of new chelators that are able to sensitize the luminescence of lanthanide ions. It is well known that aryl ketones are efficient antennas for Ln luminescence, but to enhance their binding ability to the Ln^{3+} metal one could

consider appending an electron rich phosphine oxide group to the aryl ketone of choice. This structural change may increase quantum yield values of the complexes simply by making a complex that is more kinetically stable. To increase the lifetime of the excited state, one could consider adding steric bulk to the aryl ketone in the form of weak electron donors such as alkyl groups. These structural changes should not perturb the energy of the excited states of the ligand, yet the presence of steric bulk in the second-coordination sphere of the metal could act to protect the metal from competitive ligands (e.g. water, solvent) that could quench metal emission.

Future work planned for our group involves the synthesis of β -carbonyl phosphine oxide compounds that bear electron-rich, yet sterically undemanding groups on the phosphine oxide moiety with bulky substituents on the aryl ketone. We intend to study the effect of these structural changes on the solution dynamics and Ln luminescence properties of the resultant complexes. The influence of solvent coordination ability (e.g. CHCl_3 vs. CH_3CN vs. MeOH vs. H_2O) on the photophysical properties of the complexes is another variable that can be explored in the future. This is especially important since the application of ligands bearing a β -carbonyl phosphine group to the separation of lanthanide metals will likely occur using solvents other than acetonitrile.

Conflict of interest statement

There are no conflicts to declare.

Acknowledgements

We thank many sources within GVSU for financial support: the Chemistry Department Weldon Fund, CSCE, CUSE (S^3 and Kindschi Fellowships, G. Sands), and the CLAS Dean's Office (Horiba fluorimeter). We are grateful to the National Science Foundation for financial support for students (REU CHE-1559886, E. Leach; RUI CHE-2102576) and instrumentation (MRI CHE-1725699: JEOL 400 NMR, MRI CHE-1919817: Agilent UHPLC-MS). We thank the Barry M. Goldwater Foundation for a Fellowship to G. Sands, and the United States Air Force Summer Faculty Fellowship program (S. Biros). Finally, we are grateful to Prof. Eric Werner (The University of Tampa) and Prof. Ana de Bettencourt-Dias (University of Nevada, Reno) for advice and helpful conversations. We also thank both reviewers of this manuscript for their insightful and helpful comments.

Literature Cited

1. Atwood, D. A. *The Rare Earth Elements: Fundamentals and Applications*. 1st ed.; John Wiley & Sons Ltd: Chichester, 2012.
2. Bünzli, J.-C. G., *Eur. J. Inorg. Chem.* **2017**, 5058-5063.
3. Girard, P.; Namy, J. L.; Kagan, H. B., *J. Am. Chem. Soc.* **1980**, *102*, 2693-2698.
4. Wang, Y.-H.; Yang, Q.; Walsh, P. J.; Schelter, E. J., *Org. Chem. Front.* **2022**, *9*, 2612-2620.
5. Werner, E. J.; Datta, A.; Jocher, C. J.; Raymond, K. N., *Angew. Chem. Int. Ed.* **2008**, *47*, 8568-8580.
6. Lux, J.; Sherry, A. D., *Curr. Opin. Chem. Biol.* **2018**, *45*, 121-130.
7. de Bettencourt-Dias, A. *Luminescence of Lanthanide Ions in Coordination Compounds and Nanomaterials*. 1st ed.; Wiley: Chichester, 2014; p 384.
8. Gai, S.; Li, C.; Yang, P.; Lin, J., *Chem. Rev.* **2014**, *114*, 2343-2389.
9. Zhu, Z.; Guo, M.; Li, X.-L.; Tang, J., *Coord. Chem. Rev.* **2019**, *378*, 350-364.
10. Gould, C. A.; McClain, K. R.; Reta, D.; Kragoskow, J. G. C.; Marchiori, D. A.; Lachman, E.; Choi, E.-S.; Analytis, J. G.; Britt, R. D.; Chilton, N. F.; Harvey, B. G.; Long, J. R., *Science* **2022**, *375*, 198-202.
11. Godfrin, C.; Ferhat, A.; Ballou, R.; Klyatskaya, S.; Ruben, M.; Wernsdorfer, W.; Balestro, F., *Phys. Rev. Lett.* **2017**, *119*, 187702.
12. Gutfleisch, O.; Willard, M. A.; Brück, E.; Chen, C. H.; Sankar, S. G.; Liu, J. P., *Adv. Mater.* **2011**, *23*, 821-842.
13. Horwitz, E. P.; Kalina, D. C.; Diamond, H.; Vandegrift, G. F.; Schulz, W. W., *Solvent Extr. Ion Exch.* **1985**, *3*, 75-109.
14. Leach, E. G.; Shady, J. R.; Boyden, A. C.; Emig, A.; Henry, A. T.; Connor, E. K.; Staples, R. J.; Schaertel, S.; Werner, E. J.; Biros, S. M., *Dalton Trans.* **2017**, *46*, 15458-15469.

15. Ibarra, I.; Hesterberg, T. W.; Holliday, B.; Lynch, V.; Humphrey, S. M., *Dalton Trans.* **2012**, *41*, 8003-8009.
16. Pilichos, E.; Tubau, À.; Speed, S.; Font-Bardia, M.; Escuer, A.; Grabulosa, A.; Mayans, J., *Dalton Trans.* **2023**, *52*, 2485-2494.
17. Iwanaga, H., *ASTESJ* **2023**, *8*, 154-160.
18. Charbonnière, L. J.; Ziessel, R.; Montalti, M.; Prodi, L.; Zaccheroni, N.; Boehme, C.; Wipff, G., *J. Am. Chem. Soc.* **2002**, *124*, 7779-7788.
19. Zairov, R.; Dovzhenko, A.; Terekhova, N.; Kornev, T.; Zhou, Y.; Huang, Z.; Tatarinov, D.; Nizameeva, G.; Fayzullin, R. R.; Gubaidullin, A. T.; Salikhova, T.; Enrichi, F.; Mironov, V. F.; Mustafina, A., *Nanomaterials* **2023**, *13*, 438.
20. Sengupta, A.; Kadam, R. M., *Spectrochim. Acta, Part A* **2017**, *173*, 328-334.
21. Aslandukov, A. N.; Utochnikova, V. V.; Goriachiy, D. O.; Vashchenko, A. A.; Tsybarenko, D. M.; Hoffmann, M.; Pietraszkiewicz, M.; Kuzmina, N. P., *Dalton Trans.* **2018**, *47*, 16350-16357.
22. Hirai, Y.; Nakanishi, T.; Hasegawa, Y., *J. Lumin.* **2016**, *170*, 801-807.
23. Weissman, S. I., *J. Chem. Phys.* **1942**, *10*, 214-217.
24. de Bettencourt-Dias, A., *Curr. Org. Chem.* **2007**, *11*, 1460-1480.
25. Bünzli, J.-C. G., *Coord. Chem. Rev.* **2015**, *293-294*, 19-47.
26. Eliseeva, S. V.; Bünzli, J.-C. G., *Chem. Soc. Rev.* **2010**, *39*, 189-227.
27. Montalti, M.; Credi, A.; Prodi, L.; Gandolfi, M. *Handbook of Photochemistry*, 3rd ed. Taylor & Francis.
28. Parker, C. A.; Rees, W. T., *Analyst* **1960**, *85*, 587-600.
29. Crosby, G. A.; Whan, R. E.; Alire, R. M., *J. Chem. Phys.* **1961**, *14*, 743-748.
30. Tauc, J.; Grigorovici, R.; Vancu, A., *Phys. Status Solidi B* **1966**, *15*, 627-637.
31. Makuła, P.; Pacia, M.; Macyk, W., *J. Phys. Chem. Lett.* **2018**, *9*, 6814-6817.

32. Ramya, A. R.; Reddy, M. L. P.; Cowley, A. H.; Vasudevan, K. V., *Inorg. Chem.* **2010**, *49*, 2407-2415.
33. Frisch, M. J., *et al.*, *Gaussian, Inc.: Wallingford, CT, 2009*,
34. Li, R.; Keith, T.; Millam, J.; Eppinnett, K.; Hovell, L.; Gilliland, R. *Gaussview, Version 5*.
35. Arnaud Neu, F.; Böhmer, V.; Dozol, J. F.; Grüttner, C.; Jakobi, R. A.; Kraft, D.; Mauprivez, O.; Rouquette, H.; Schwing-Weill, M. J.; Simon, N.; Vogt, W., *J. Chem. Soc. Perkin Trans. 2* **1996**, 1175-1182.
36. Schuster, E. M.; Nisnevich, G.; Botoshansky, M.; Gandelman, M., *Organometallics* **2009**, *28*, 5025-2031.
37. Leach, E. G.; Kulesza, A. A.; Staples, R. J.; Biros, S. M., *Acta Cryst.* **2015**, *E71*, 523-527.
38. Zhao, X.; Huang, M.; Li, Y.; Zhang, J.; Kim, J. K.; Wu, Y., *Org. Chem. Front.* **2019**, *6*, 1433-1437.
39. Kumar, D. S.; Alexander, V., *Inorg. Chim. Acta.* **1995**, *238*, 63-71.
40. Aruna, V. A. J.; Alexander, V., *J. Chem. Soc., Dalton Trans.* **1996**, 1867-1873.
41. Carnall, W. T.; Siegel, S.; Ferraro, J. R.; Tani, B.; Gebert, E., *Inorg. Chem.* **1973**, *12*, 560-564.
42. James, S.; Kumar, D. S.; Alexander, V., *J. Chem. Soc., Dalton Trans.* **1999**, 1773-1777.
43. Babecki, R.; Platt, A. W. G.; Fawcett, J., *J. Chem. Soc. Dalton Trans.* **1992**, 675-681.
44. Bünzli, J.-C. G., *Chem. Rev.* **2010**, *110*, 2729-2755.
45. Cotton, S. *Lanthanide and Actinide Chemistry*. Wiley: 2006; p 280.
46. Binnemans, K., *Coord. Chem. Rev.* **2015**, *295*, 1-45.
47. Babecki, R.; Platt, A. W. G.; Tebby, J. C.; Fawcett, J.; Russell, D. R.; Little, R., *Polyhedron* **1989**, *8*, 1357-1360.
48. Babecki, R.; Platt, A. W. G.; Russell, D. R., *Inorg. Chim. Acta.* **1990**, *171*, 25-28.

49. Werts, M. H. V.; Jukes, R. T. F.; Verhoeven, J. W., *Phys. Chem. Chem. Phys.* **2002**, *4*, 1542-1548.
50. Tsurui, M.; Kitagawa, Y.; Shoji, S.; Ohmagari, H.; Hasegawa, M.; Gon, M.; Tanaka, K.; Kobayashi, M.; Taketsugu, T.; Fushimi, K.; Hasegawa, Y., *J. Phys. Chem. B* **2022**, *126*, 3799-3807.